RSC Advances

ROYAL SOCIETY OF CHEMISTRY

www.rsc.org/advances

Journal Name

RSCPublishing

ARTICLE

Robust Reduced Graphene-Oxide Paper Fabricated by Household Non-stick Frying pan: Large-area Freestanding Flexible Substrate for Supercapacitor†

Cite this: DOI: 10.1039/x0xx00000x

Received 00th January 2012,
Accepted 00th January 2012

DOI: 10.1039/x0xx00000x

www.rsc.org/

Yang Huang,[a] Minshen Zhu,[a] Wenjun Meng,[a] Yuqiao Fu, [a] Zifeng Wang,[a] Yan Huang,[a] Zhengxia Pei [a] and Chunyi Zhi*[ab]

Inspired by the omelette cooking, a facile, low-cost and scalable method involving readily available household non-stick frying pan is introduced to fabricate large-area freestanding reduced graphene oxide (RGO) paper. The as-fabricated RGO paper is robust enough to bear sandpaper polishing, bending/folding, hydrothermal and electrochemical deposition processes without obvious structure/performance degradation. As a demonstration, the as-obtained RGO papers were directly used as universal flexible substrates for high performance supercapacitor (SC). Thus, WO_3 and PPy, two distinctive active materials, were loaded on the RGO paper via a hydrothermal and electrodeposition process, respectively, which are two typical fabrication methods for high performance SC electrodes. The resultant WO_3- and PPy-RGO paper, acting as negative and positive electrodes, respectively, were further assembled into a flexible asymmetric supercapacitor (ASC), achieving a high energy density of 0.23 mWh cm^{-3} at a power density of 7.3 mW cm^{-3} when normalized to the whole volume. Moreover, benefiting from the robust flexible RGO substrate, performance of the ASC showed great stability under different bending angle and even after hundreds of times bending/folding. These exciting results demonstrate our robust RGO paper is an ideal universal substrate for different active materials synthesized via various processing methods, showing great potential in all-solid energy storage system with excellent flexibility and robustness.

1. Introduction

The blooming of personal electronics, especially the ever-increasing consumption of wearable electronics, has prompted the development for lightweight, flexible, and highly efficient energy storage devices.[1, 2] In accordance with this trend, a variety of flexible all-solid supercapacitors (SCs) combined with exceptionally long cycle life, enhanced high power and energy density, good operational safety and environmental benign nature have been designed and fabricated currently.[3, 4] For high performance flexible SCs, special attention has be dedicated to the design of flexible electrodes, and two main kinds of strategies have been developed, such as: i) fabricating flexible hybrid electrodes of active materials;[5, 6] ii) fabricating freestanding conductive substrates to support active materials.[7, 8] Compared with hybrid electrodes, the use of substrate is more attractive, not only because of their low cost and high flexibility but also, more importantly, because it is more universal and could open up the possibility to support any upcoming active material with enhanced performance via different processing methods.

Recently, metals,[4] carbon based materials,[9] textiles,[10] sponges[11] and even conventional paper[12, 13] have been used as substrates to fabricate high performance flexible SCs. Among them, graphene based materials, one of the most commonly reported carbon materials lately, have attracted significant attentions owing to its outstanding electronic, mechanical, and thermal properties,[14, 15] leading to a wide range of applications such as conducting transparent electrodes,[16] electrochemical batteries,[17] sensors,[18] and SCs as well.[19] Thanks to its 2-dimensional properties, these graphene based materials can be easily assembled into macroscopic paper-like structure, an ideal flexible substrate for loading active materials. Generally, there are two main approaches to obtain graphene based paper, one is direct production by using reduced graphene oxide (RGO),[6, 20] the other is relying on post-reduction of pre-fabricated GO paper.[21] However, current strategies for the production of freestanding RGO paper substrate are far from satisfactory,

since they are usually time consuming (*e.g.* membrane filtration)[6] and require custom accessories or delicate equipment (*e.g.* electrophoretic deposition and chemical vapor deposition (CVD)),[22, 23] which may impede their further development in large-scale fabrication. Obviously, the largest obstacle is the achievement of a large-area RGO paper via a simple method with high efficiency.

Herein, we develop an ingenious method to fabricate a large-area freestanding RGO paper by using household utensils, which is demonstrated to be a facile, low cost and scalable method inspired by cooking an omelette. After successful post-reduction, the obtained RGO paper exhibit excellent mechanical and electrical properties, as well as great compatibilities to different active materials and processing methods, which can be directly used as robust substrate for high performance SC. As a demonstration, two distinctive active materials (WO_3 and PPy) were loaded on RGO substrate perfectly via hydrothermal and electrodeposited methods, two typical synthesis methods for SC electrodes. These two resultant flexible electrodes were further assembled into a high performance all-solid asymmetric supercapacitors (ASCs) achieving a high energy density of 0.23 mWh cm^{-3} at a power density of 7.3 mW cm^{-3}. What's more, this ASCs showed no degradation under different bending angle and remained stable even after hundreds of times bending, together with excellent cycling stability (retaining 99.4% after 2000 cycles). Therefore, the RGO paper, with excellent flexibility and robustness, is an ideal universal substrate for various active materials synthesized via different processing methods, showing great potential for various portable/wearable electronics.

2. Experimental Section

2.1 Fabrication of the RGO paper

GO was prepared from purified natural graphite by using a modified Hummers method.[24] The suspension of GO sheets was obtained by ultrasonic exfoliation of the as-prepared GO in deionized (DI) water, followed by centrifugation at 5000 rpm for 10 min to remove non-exfoliated sheets.

The ingenious fabrication of large area free standing RGO paper is inspired by the daily cooking of an omelette, as shown in the schematic demonstration of Fig. 1A. Pour adequate GO suspension (5 mg mL^{-1}, 100 mL), a viscous liquid similar to egg liquid, directly into a common household non-stick frying pan (IKEA, with a diameter of 20 cm), spreading them evenly with a spatula. Place the frying pan on an induction cooker and keep it under appropriate heating (60W, 80 to 90 °C) until GO suspension is dried, normally required 2-3 hours. The heating temperature is suggested to be maintained under 100 °C, since small pores will form if the suspension solution is boiling. Then, the GO paper was easily peeled off form the frying pan and reduced into RGO paper by immersing into a hydrohalic acid (HI) solution in a sealed cuvette.[21] Finally, the large area freestanding RGO paper was annealed at 750 °C under an argon flow of 50 mL min^{-1} for 2 h, which was employed for elimination of the introduced sub-products (I^- ions), meanwhile providing extra reduction.

2.2 Fabrication of WO_3- and PPy-RGO paper

The RGO paper was first cut into appropriate size (*e.g.* 5 cm × 2 cm) and polished with sandpaper (P1000) in order to obtain a unique fish scale-like structure. The pre-treated paper was washed with DI water and dried prior to use.

WO_3-RGO paper electrode was prepared by a hydrothermal method while using RGO paper as a substrate according to the previous report.[25] 10 mL 0.3 M HCl was slowly added into the 10 mL solution containing 0.6 g $Na_2WO_4 \cdot 2H_2O$, and then, 0.6 g NaCl was added into the solution. Subsequently, the RGO paper was immersed in the resultant solution and transferred into a Teflon-lined stainless autoclave, then heated at 180 °C for 12 h. After autoclave cooled down to room temperature, the RGO paper was taken out, rinsed with DI water and dried prior to use. The precipitates were collected by centrifugation (5000 rpm), washed by DI water and absolute ethanol several times, and finally dried overnight.

PPy-RGO paper electrode was prepared by electrodeposited method while using a three-electrode configuration with RGO paper as working electrode, platinum mesh as counter electrode, and Ag/AgCl as reference electrode. Briefly, the electrodeposition solution contained 300 μL distilled pyrrole monomer, 0.1 M p-toluenesulfonic acid, 0.3 M sodium dodecylbenzenesulfonate and 60 mL DI water. A constant voltage of 0.8 V was used during the deposition process, and lasted for 90 s. Then the PPy-RGO paper was washed with DI water and dried prior to use.

2.3 Assemble of WO_3-RGO//PPy-RGO ASC

The WO_3- and PPy-RGO paper, acting as negative and positive electrodes, were assembled into an ASC by using PVA-H_2SO_4 as solid electrolyte. The PVA-H_2SO_4 gel electrolyte was firstly prepared by dissolving PVA powder (6 g) in DI water (60 mL) and H_2SO_4 (6 g). The mixture was heated to 150 °C with vigorous stirring until a transparent solution formed. Then, the RGO based electrodes were coated with a thin layer of PVA-H_2SO_4 gel electrolyte and dried in vacuum at room temperature. After that, coated another thin layer of gel electrolyte on one of the resultant electrodes, pasted the other onto it gently and dried in air. Thus, a flexible all-solid ASC was obtained.

2.4 Materials characterization and electrochemical measurements

Morphology of the samples was investigate by environmental scanning electron microscope (ESEM, FEI/Philips XL30). X-ray diffraction (XRD) patterns were collected with a BRUKER D2 PHASER diffractometer equipped with CuK_α irradiation (λ = 1.54184Å, 30 kV and 10 mA). X-ray photoelectron spectroscopy (XPS) measurements were performed on an ESCALAB 220i-XL electron spectrometer with monochromatic Al K_α X-ray radiation and a hemispherical electron energy analyzer. Raman spectra were excited with a laser of 523 nm and record with Labram spectrometer. The

electrical conductivity of the RGO paper was measured by a standard four-probe method. Mechanical property measurements were performed on strips of the papers with an Instron 5661 tester (tensile rate = 0.020 mm min^{-1}). Sample widths were measured by vernier caliper, while the thickness was measured on the fracture edges with SEM. Electrochemical measurements including cyclic voltammetry (CV) curves, galvanostatic charge/discharge curves, electrochemical impedance spectroscopy (EIS, 100 KHz-0.05 Hz) were conducted on a CHI 760e electrochemical workstation (CH Instruments Company). The electrochemical performance of individual electrodes was investigated using a conventional three electrode system (Pt mesh as counter electrode and Ag/AgCl as reference electrode) in 1 M H_2SO_4 prior to the assembling of ASC. The performance of ASC was measured using a two-electrode method.

2.5 Calculations

The areal (C_s, F cm^{-2}) and specific (C_m, F g^{-1}) capacitance of the positive or negative electrode in three electrode configuration were calculated from corresponding charge/discharge curves at different current densities according to the equation (1):

$$C_s = I\Delta t / s\Delta V \text{ or } C_m = I\Delta t / m\Delta V \quad (1)$$

Where I (A) is the discharge current, Δt (s) is the discharge time, s is the specific area (cm^2), m (g) is the total mass of the electrode, and ΔV (V) is the discharge voltage range (excluding iR drop).

The capacitance values of the ASC were calculated from the corresponding CV curves at different scan rates according to the equation (2):

$$C_{device} = \frac{1}{\nu(V_f - V_i)} \int_{V_i}^{V_f} I(V)\mathrm{d}V \quad (2)$$

Where C_{device} is denoted as the capacitance contribute from the asymmetric electrodes, ν is the scan rate (V s^{-1}), V_f and V_i are the integration potential limits of the voltammetric curve and $I(V)$ is the voltammetric discharge current. Specific capacitance were calculated based on the areal or the whole volume of the device according to the following equation:

$$C_s = C_{device} / A \text{ or } C_V = C_{device} / V \quad (3)$$

Where C_S (F cm^{-2}) and C_V (F cm^{-3}) refer to the areal capacitance and volumetric stack capacitance of the ASC, respectively. A and V are the total area (cm^2) and volume (cm^3) of the device. The areal capacitance was calculated based on the entire projected surface area of the device. The volumetric stack capacitance was calculated by taking into account the whole device, including solid electrolyte. Charge balance between negative and positive electrodes is obtained by the equation: $C_- V_- = C_+ V_+$, where C_- and C_+ are the capacitance of negative and positive electrodes respectively, and V_- and V_+ are the potential window of negative and positive electrodes respectively.

The volumetric energy density of the ASC was obtained from the following equation:

$$E_V = \frac{1}{2} \times C_V \times \frac{(\Delta V)^2}{3600} \quad (4)$$

where E_V (Wh cm^{-3}) is the volumetric energy density, C_V is the volumetric stack capacitance obtained from equation (3). ΔV (V) is the discharge voltage range.

The power density of the device was calculated from the following equation:

$$P_V = \frac{E_V}{\Delta t} \times 3600 \quad (5)$$

Where P_V (W cm^{-3}) is the volumetric power density, E_V is the volumetric energy density obtained from equation (4) and Δt (s) is the discharge time.

3. Results and Discussion

3.1 Fabrication of large area freestanding RGO Paper

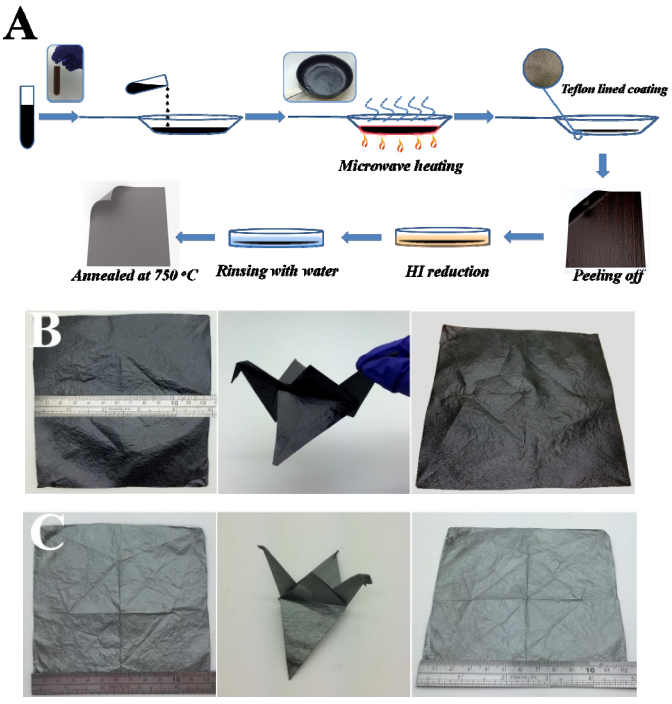

Fig. 1 (A) Schematic representation of a proposed fabrication process of the large-area freestanding RGO paper via household utensils. Homogeneous GO suspension solution is directly poured into a non-stick frying pan, and dried with moderate heating. After the suspension is dried, the GO paper is easily peeled off and reduced into RGO paper by HI solution and thermal annealing. (B) Photograph of a large-area freestanding dark brown GO paper (left), folded into an origami crane (centre) and the extension GO paper after origami crane folding (right). (about 12 cm × 12 cm, 144 cm^2) (C) Photograph of a large-area freestanding silver RGO paper (left), folded into an origami crane (centre), and the extension RGO paper after origami crane folding (right). (about 12 cm × 12 cm, 144 cm^2)

As shown in Fig. 1 A, when the water keeps evaporating under continuous heating and lead to a higher and higher GO concentration, the supersaturated GO sheets float on the surface will aggregate together and self-stack into a thin film because of the increasing sheet-to-sheet interaction, thus forming a layer by layer GO paper by the end. Thanks to the Teflon lined coating, the dried dark brown round-shape GO paper can be easily peeled off from the frying pan.(Fig. S1†) Then, this GO paper can be easily reduced into a highly conductive RGO paper by HI solution and thermal annealing. Based on the ingenious method, large-area freestanding flexible RGO papers with a variety of sizes and thicknesses can be obtained by just changing non-stick pans with different sizes or simply adjusting the volume and concentration of GO suspension. As a demonstration, a GO paper with a surface area of 144 cm^2 was made and could be folded into an origami crane. After unfolding, amazingly, there were only several creases left on the paper. (Fig. 1B) Then this pristine GO paper was reduced into RGO paper by the aforementioned methods. The RGO paper demonstrated similar flexibility and toughness with the pristine GO paper, showing no defects even after complex folding.(Fig. 1C) While comparing to other reported fabrication methods for RGO paper,[22, 26-30] our ingenious approach has more advantages: i) convenient and easy to scale up, the equipment is common household non-stick pan, which are readily available, and with the possibilities to fabricate RGO papers with any sizes; ii) time saving, water evaporation of GO suspension exhibits a satisfactory efficiency, especially comparing with traditional time consuming vacuum assisted flow-filtration method; iii) cost-effective, since the pan can be readily reused after cleaning, the cost is extremely low.

3.2 Characterization

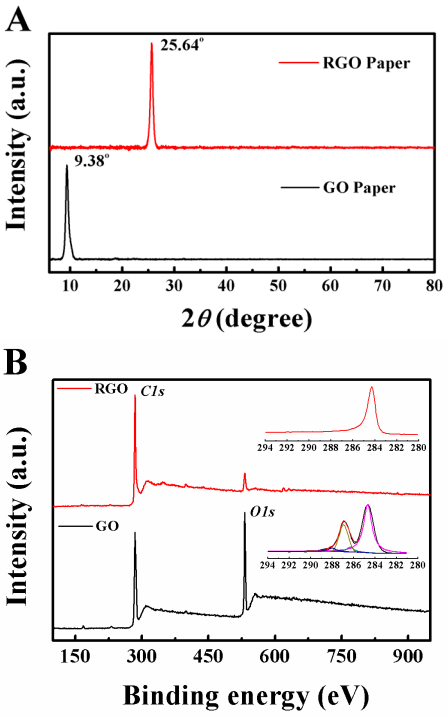

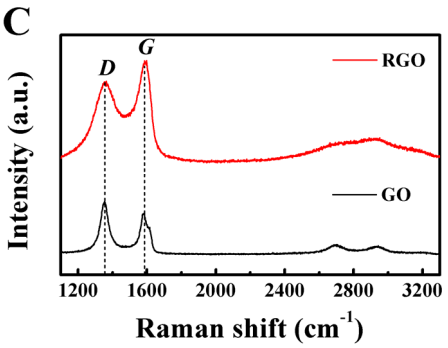

Fig. 2 (A) XRD patterns of GO and RGO papers. (B) High-resolution XPS spectra (C1s) of GO and RGO papers. (The position of C-C/C=C, C-O, C-O-C, and C=O/O-C=O is 284.7 eV, 286.3 eV, 286.9 eV and 288.3 eV.) (C) Raman spectra of GO and RGO paper collected with a laser of 532 nm.

The deoxygenation and interlaminar consolidation of the as-prepared papers was proven by the detailed characterization of XRD and XPS. As shown in Fig. 2A, the XRD pattern of GO paper presents a diffraction peak at 2θ = 9.38°, suggesting a larger interlayer spacing (0.94 nm) due to the presence of oxygen-containing functional groups (*e.g.* epoxy and hydroxyl groups) attached to the GO sheet surface and molecules of water coming from the harsh oxidation applied.[31] In case of RGO paper, the diffraction peak of RGO is shifted to 25.64°, becoming narrower and sharper, not only indicating a significant reduction of the interlayer distance (0.35 nm) owing to the elimination of oxygen-containing groups, but also revealing more regular packing of graphene layers with a longer correlation length due to the coalescence of graphene sheets.[21] High resolution of C1s peaks in the XPS of the RGO paper also proves that oxygen-containing groups have been removed.(Fig. 2B) Deconvolution of C1s spectrum in the pristine GO paper reveals that it consists of two main components arising from C-O (hydroxyl and epoxy, ~286.3 eV) and C-O-C (~286.9 eV) and one minor component C=O/O-C=O (carbonyl, ~288.3 eV). After the post-reductions, it is clear that majority of oxygen-containing groups in pristine GO paper are almost all removed and the C-C/C=C bonds become dominant (~284.7 eV) in the RGO paper, as shown by the one single peak with a small tail in the higher binding energy region in Fig. 2B. The surface C/O atomic ratio detected by XPS is ~2.8 for the pristine GO paper and is increased to ~12.5 after post-reductions, strongly indicating the complete elimination of oxygen groups.

The removal of oxygen-containing groups leads to greater connectivity among the existing graphitic domains by formation of new sp^2 clusters,[32] which can also be followed by Raman spectroscopy. G-band (at 1585 cm^{-1}) is well-known to be the characteristic of the sp^2-hybridized carbon-carbon bonds in graphene.[33, 34] Meanwhile, the presence of the D-band (at 1350 cm^{-1}) indicates the structural imperfections induced by the attachment of oxygen-containing functional groups on the carbon basal plane.[34] As a result, I_D/I_G ratios is widely used to provide structural information of GO with different degree of reduction, while a high I_D/I_G is related to the presence of

disorder carbon and/or functionalities attached to graphene sheets. Compared with GO paper, the intensity of D-band peak in RGO paper reduced obviously and the I_D/I_G ratio decreased notably from 1.31 to 0.82, suggesting the extensive repairing of defects created by the attachment of oxygen groups.

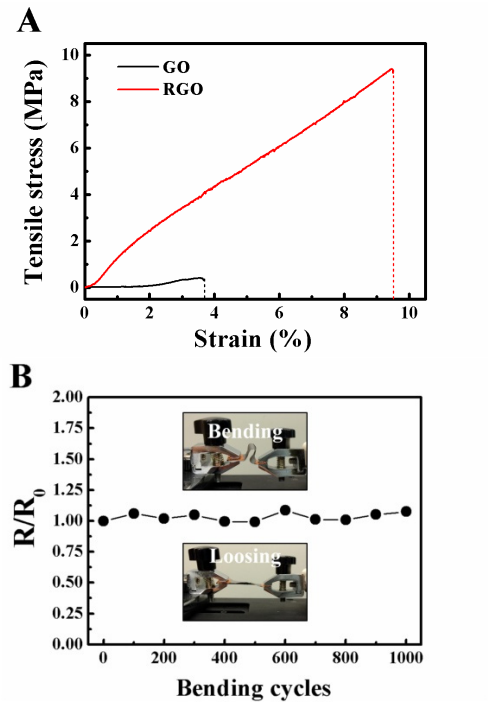

Fig. 3 (A) Tensile measurements of the GO and RGO papers. (B) Electrical resistance of a RGO paper (about 4 cm × 6 cm, 24 cm^2) with bending test: R_0 and R correspond to the original resistance and resistance after bending. Inset shows the bending (above) and loosing (under) film.

Owing to the restoration of sp^2 carbon network in GO sheets and the decrease of interlayer distance, as revealing in structural characterization, the interaction among reduced GO sheets in RGO paper is increased; thus, the electrical conductivity and mechanical strength of RGO paper are greatly improved. Conductivities of the RGO paper were measured in a co-lineal four point probes method and high value of electrical conductivity was achieved by our progressive reduction, reaching as high as 203.7 S cm^{-1}. Due to the increase neighbouring coalescence interaction between RGO sheets, the RGO paper has a modulus of 1.65 GPa and a strength of 9.41 MPa, which is 11 times and 21 times more than that of the pristine GO paper (modulus 0.13 GPa, strength 0.41 MPa).(Fig. 3A) Accordingly, RGO paper presents outstanding flexibility and toughness as shown in Fig. 1C. To further investigate whether the good electrical conductivity of RGO paper is in agreement with its robust body, cycled bending tests of the resistance were operated by a designed stepper motor. It is very impressive that the resistance showed no observable change after 1000 times bending,(Fig. 3B) indicating that the good electrical conductivity was integrated with its robust body. Good electrical conductivity, together with excellent mechanical strength, are important to apply the flexible substrates to high-performance SC electrode. Because they can ensure the substrate bears various post-treatments and fabrication processes.[35] Based on the above demonstrations, our RGO paper should be an ideal substrate for SC.

3.3 Universal robust substrate for high-performance SC electrode

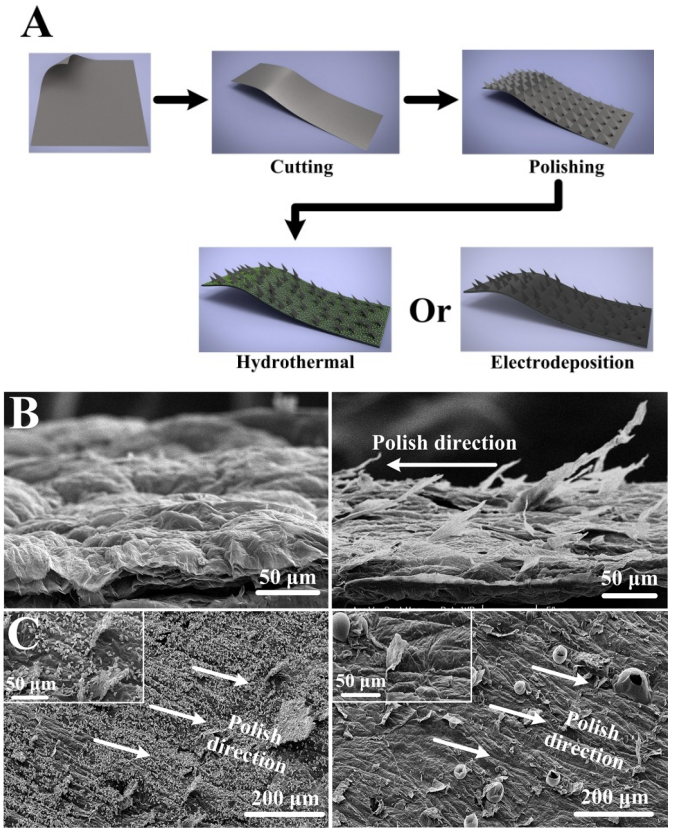

Fig. 4 (A) Schematic illustration of the fabrication process of WO_3- and PPy-RGO electrodes. One large free-standing flexible RGO substrate is firstly cut into appropriate size and polished with sand paper in one direction. After that the processed substrate is treated with hydrothermal or electrodeposited method, in order to load enough active materials on its surface. (B) SEM images showing the RGO paper before polishing (left) and after polishing (right). (C) SEM images of WO_3-RGO (left) and PPy-RGO (right) paper electrodes. Insets are the high resolution images.

To further investigate the robust RGO paper as a universal substrate for different active materials synthesized via different processing methods, two different kinds of electrodes with well-designed structures are fabricated by hydrothermal (WO_3) and electrodeposited (PPy) methods, respectively, which are two representative processing methods for high-performance SCs.[4, 36](Fig. 4A) One large free-standing flexible RGO paper is firstly cut into appropriate size (*e.g.* 5 cm × 2 cm, 10 cm^2), and then polished with sandpaper along one direction. Hence, the smooth surface of RGO paper becomes rougher and exhibits a unique fish scale-like structure, as shown in Fig. 4B. These micro fish scale-like RGO sheets, as torn off from the bulk self-stack RGO paper, ensure more active materials could be loaded on the substrate, which may result in a better electrochemical

performance. Benefiting from the robust features, the polished RGO paper can bear both hydrothermal and electrodeposited methods, turning the conductive substrate into a flexible electrode. As shown in the Fig. 4C, after hydrothermal treatment, numerous nano particles, which were characterized to be WO_3, (JCPDS NO.75-2187, Fig. S2†) anchored both on the rough surface and the fish scale-like sheets; while after electrodeposition, the scratches and steps were alleviated obviously, since a thin layer of PPy, one typical conductive polymer, was successfully coated on the rough surface.

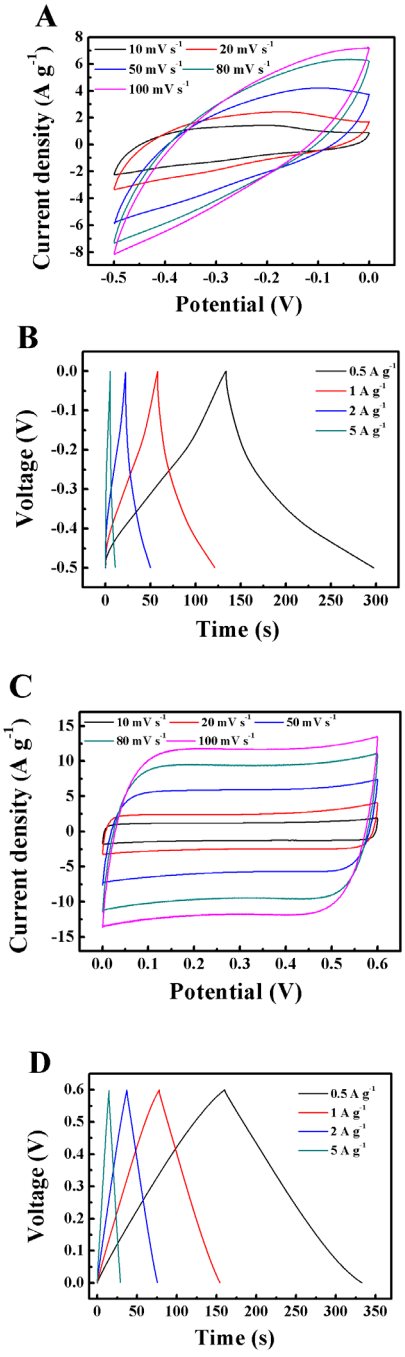

Fig. 5 Electrochemical performance of hydrothermal WO_3-RGO paper electrode in a three-electrode system: (A) CV at different scan rates of 10, 20, 50, 80, and 100 mV s^{-1} (from inner to outer). (B) Galvanostatic charge/discharge curves at different current densities of 0.5, 1, 2, and 5 A g^{-1}. Electrochemical performance of electrodeposited PPy-RGO paper electrode in a three-electrode system: (C) CV at different scan rates of 10, 20, 50, 80, and 100 mV s^{-1} (from inner to outer). (D) Galvanostatic charge/discharge curves at different current densities of 0.5, 1, 2, and 5 A g^{-1}.

Due to their excellent conductivity and integrated structure, the free-standing WO_3 loaded and PPy coated RGO papers can be directly used as SC electrodes. A three electrode test configuration was employed to evaluate the electrochemical performance of both WO_3- and PPy-RGO paper electrodes. Fig. 5A&C shows CV loops of the both electrodes in the range of 10-100 mV/s. The CV curve of WO_3-RGO electrode is deviated from a rectangular shape, which can be attributed to the relatively large resistance, while the CV curve of PPy-RGO electrode is in rectangular at the applied scan rates, indicating an excellent capacitive behaviour and a low resistance.[37] The charge and discharge curves at different charge current are shown in Fig. 5B&D. The deviation of charge-discharge curves from the linear voltage-time relation of WO_3-RGO electrode indicates pseudo-capacitive behaviour resulting from redox reactions,[38] whereas the curves of PPy-RGO electrode are highly linear and symmetrical, suggesting a very good capacitive behaviour.[39] Besides, no obvious *iR* drop is observed for any of the curves, indicating a rapid I-V response and an excellent electrochemical reversibility.[6] The specific capacitance is calculated to be 123.4 F g^{-1} (WO_3-RGO) and 127.5 F g^{-1} (PPy-RGO) at a current density of 1 A g^{-1}, corresponding to 71 mF cm^{-2} and 80 mF cm^{-2}.

3.4 Assembly of flexible all-solid state ASC

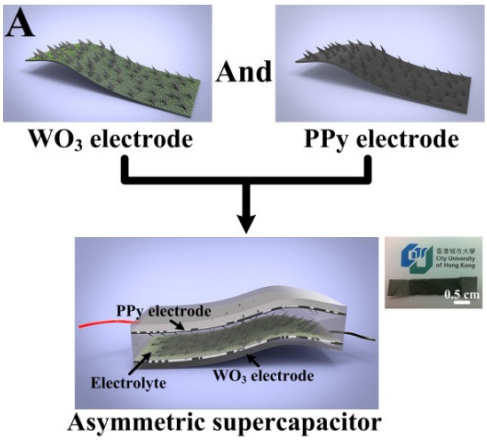

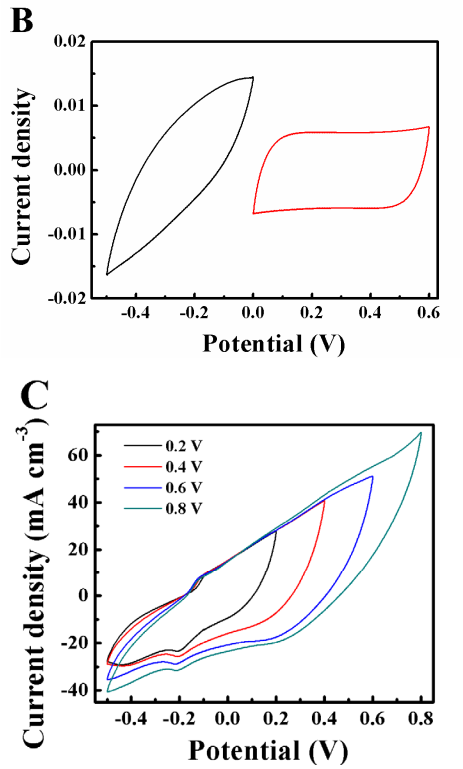

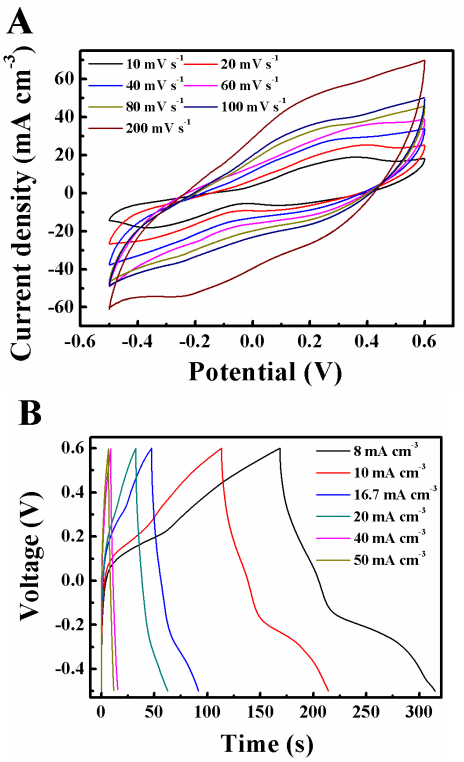

Fig. 6 (A) Schematic illustration of the fabrication process of WO_3-RGO//PPy-RGO ASC. Inset is photograph of the all-solid asymmetric device. (B) Comparative CV of WO_3- and PPy-RGO paper electrodes in a three-electrode system at a scan rate of 100 mV s^{-1}. (C) CVs of the WO_3-RGO//PPy-RGO ASC at different potential windows at a scan rate of 100 mV s^{-1}.

The robust freestanding RGO paper, which is compatible with distinctive active materials and can bear various processing methods perfectly, is an ideal substrate for flexible SC electrodes. To further demonstrate its promising application in high performance power devices with excellent flexibility, an all-solid state ASC was further fabricated by assembling the as-prepared WO_3- and PPy-RGO papers as negative and positive electrodes, respectively. The mass ratio of the two electrodes fixed to 1.24, in order to achieve a charge balance between the negative and positive electrodes.(Fig. 6A)

The stable operating potential windows for WO_3- and PPy-RGO electrodes are -0.5～0 V and 0～0.6 V, respectively.(Fig. 6B) The cell voltage can be expressed as the sum of potential range of the electrodes, and consequently, the asymmetric device is expected to work within a voltage window of -0.5～0.6 V. A series of CV measurements under different voltage windows are shown in Fig. 6C. The device exhibits a stable potential window even up to 1.3 V, which exceeds the theoretical decomposition voltage of water (1.23 V) and could be ascribed to the high overpotential of hydrogen evolution on the electrode.[40]

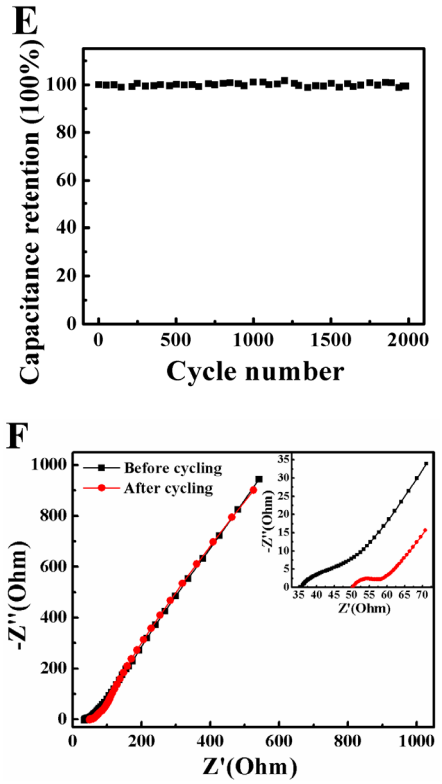

Fig. 7 Electrochemical performance of the WO_3-RGO//PPy-RGO ASC: (A) CVs at different scan rates of 10, 20, 40, 60, 80, 100, and 200 mV s^{-1} (from inner to outer). (B) Galvanostatic charge/discharge curves at different current densities of 8, 10, 16.7, 20, 40, and 50 mA cm^{-3}. (C) CVs of WO_3-RGO//PPy-RGO ASC at a scan rate of 100 mV s^{-1} with different bending angles (an inward ~ 180° bending angle). (D) Ragone plots of WO_3-RGO//PPy-RGO ASC based on the whole volume. (E) Capacitance retention ratio as a function of cycle numbers at applied current of 8.3 mA cm^{-3}. (F) Nyquist plots in the frequency range of 0.05 Hz to 100 kHz before and after 2000 cycles. The inset shows an enlarge EIS.

CV curves at different scan rates (ranging from 10 to 200 mV s^{-1}) are collected in order to evaluate the performances of WO_3-RGO//PPy-RGO ASC, as shown in Fig. 7A. The assemble full cells exhibit quasi-rectangular CV curves at low scan rates, which is attributed to the combination of the non-rectangular curves of WO_3 and rectangular curves of PPy, agreeing with a good capacitive behaviour.[41] Moreover, the CV curve still remain symmetrical even at a high scan rate of 400 mV s^{-1},(Fig. S3†) indicating the good reversibility of electrochemical processes.[40] The charge-discharge curves show symmetric charge and discharge process, and the deviation from linear curve is attributed to the pseudo-capacitive behaviour of WO_3-RGO. The volumetric stack capacitance of the ASC was calculated to be 1.31 F cm^{-3} at a scan rate of 10 mV s^{-1}, which is much larger than the values reported for graphene (0.42 F cm^{-3})[42], TiN (0.33 F cm^{-3})[43] SC and H-TiO_2@MnO_2//H-TiO_2@C (0.7 F cm^{-3})[44] all-solid ASC. Correspondingly, the area capacitance was 65.7 mF cm^{-2}, which was higher than the graphene-cellulose paper based SC (47 mF cm^{-2})[20]. Noteworthy, compared with many other reported graphene based planar film or paper,[6, 20, 42] our RGO paper is merely acting as a highly conductive flexible substrate and its contribution to the capacitance is very limited,(Fig. S4†) which can eliminate unnecessary distractions of capacitive performance and provide accurate evaluation of the loaded active materials.

As previous demonstration, the RGO substrate exhibits outstanding flexibility and toughness. Thus, it is predictable that the ASC based on the RGO electrodes has great potential as flexible power source. As shown in Fig. 7C, the perfectly overlapped CV curves at different bending angles indicate that the ASC can be bent to a large extent without degrading the performance. Moreover, even after folded and unfolded to 180° over 200 times, the CV curves does not show an obvious change.(Fig. S5†) Ragone plot, showing energy and power densities (normalized to the whole device volume), is given in Fig. 7D. Significantly, our ASC possesses an high volumetric energy density of 0.23 mWh cm^{-3} at a power density of 7.3 mW cm^{-3}, which is comparable with or better than those of previously reported flexible ASC or SCs, such as hydrogenated TiO_2@MnO_2//TiO_2@C-based ASC (0.30 mWh cm^{-3}),[44] MnO_2/carbon particles-based SC (0.09 mWh cm^{-3}),[45] and graphene-based SC (0.06 mWh cm^{-3}).[42] Besides, our device shows remarkable cycling stability with a high capacitance retention of 99.4% over 2000 cycles at 8.3 mA cm^{-3}, which is significant to the practical application. This outstanding cycling performance is highly competitive with those other reported ASCs, such as $Co(OH)_2$//activated carbon(93% after 1000 cycles),[38] graphene/MnO_2//activated carbon nanofiber (97% retention after 1000 cycles),[6] MnO_2//activated carbon (96% retention after 1000 cycles),[46] MnO_2//functional mesoporous carbon nanotubes (90% retention after 1000 cycles).[47] EIS was used to investigate the resistance change of the ASC before and after the cycling test. After 2000 cycles, nearly no change was observed for R_{ct} (Ω), and only a slight increase of R_s from 36 to 50 Ω was observed. These EIS results further demonstrate the exceptional stability of our flexible ASC, which is attributed to the robust RGO substrate.

4. Conclusions

In summary, as inspired by cooking an omelette, a large area freestanding pristine GO paper was firstly fried by using a non-stick frying pan. Followed by post-reductions, the GO paper was reduced into RGO paper with excellent electrical and mechanical properties, as well as outstanding flexibility and robustness. In particular, this ingenious method can fabricate RGO papers with a variety of sizes and thicknesses just by simply changing the frying pan or the concentration of the GO solution. The as-fabricated RGO papers are very robust, being able to bear sandpaper polishing, bending, folding, hydrothermal and electrochemical deposition processes without any structure/performance degradation. As a demonstration, two flexible RGO-based electrodes were fabricated via hydrothermal and electrodeposited methods with WO_3 and PPy as active materials, respectively. The as-obtained WO_3- and PPy-RGO electrodes were further assembled into an all-solid ASC, which achieved a high energy density of 0.23 mWh cm^{-3} at a power density of 7.3 mW cm^{-3} and an outstanding retention

rate of 99.4% after 2000 cycles. In addition, benefiting from the robust features of RGO paper, the flexible all-solid ASC possesses great deformation tolerance. Consequently, the robust RGO paper, as developed by the facile, low-cost and scalable method, can be applied to fabricate high performance flexible power source, showing great potential for portable meanwhile wearable electronics.

Acknowledgements

This research was supported by the Early Career Scheme of the Research Grants Council of Hong Kong SAR, China, under Project Numbers CityU 9041977, the Science Technology and Innovation Committee of Shenzhen Municipality (Grant Number R-IND4901), and a grant from the City University of Hong Kong.

Notes and references

[a] *Department of Physics and Materials Science, City University of Hong Kong, 83 Tat Chee Avenue, Kowloon, Hong Kong. E-mail: cy.zhi@cityu.edu.hk; Fax: 852-3442-0538; Tel:852-3442-7891*

[b] *Shenzhen Research Institute, City University of Hong Kong, Shenzhen, P. R. China*

† Electronic Supplementary Information (ESI) available. See

DOI: 10.1039/b000000x/

1 Z. Liu, J. Xu, D. Chen and G. Shen, *Chem. Soc. Rev.*, 2015, **44**, 161-192.

2 G. Shen, L. Liao, C. Zhou and Y. Bando, *J. Mater. Chem. C*, 2014, **2**, 1176-1177.

3 Z. Zhang, J. Deng, X. Li, Z. Yang, S. He, X. Chen, G. Guan, J. Ren and H. Peng, *Adv. Mater.*, 2015, **27**, 356-362.

4 Y. Huang, J. Tao, W. Meng, M. Zhu, Y. Huang, Y. Fu, Y. Gao and C. Zhi, *Nano Energy*, 2015, **11**, 518-525.

5 W. Tian, X. Wang, C. Zhi, T. Zhai, D. Liu, C. Zhang, D. Golberg and Y. Bando, *Nano Energy*, 2013, **2**, 754-763.

6 Z. Fan, J. Yan, T. Wei, L. Zhi, G. Ning, T. Li and F. Wei, *Adv. Funct. Mater.*, 2011, **21**, 2366-2375.

7 J. Tao, N. Liu, L. Li, J. Su and Y. Gao, *Nanoscale*, 2014, **6**, 2922-2928.

8 S. Wang, N. Liu, J. Tao, C. Yang, W. Liu, Y. Shi, Y. Wang, J. Su, L. Li and Y. Gao, *J. Mater. Chem. A*, 2015, **3**, 2407-2413.

9 R. Ma, X. Liu, J. Liang, Y. Bando and T. Sasaki, *Adv. Mater.*, 2014, **26**, 4173-4178.

10 X. Lu, T. Zhai, X. Zhang, Y. Shen, L. Yuan, B. Hu, L. Gong, J. Chen, Y. Gao, J. Zhou, Y. Tong and Z. L. Wang, *Adv. Mater.*, 2012, **24**, 938-944.

11 P. Li, Y. Yang, E. Shi, Q. Shen, Y. Shang, S. Wu, J. Wei, K. Wang, H. Zhu, Q. Yuan, A. Cao and D. Wu, *ACS Appl. Mat. Interfaces*, 2014, **6**, 5228-5234.

12 B. Yao, L. Yuan, X. Xiao, J. Zhang, Y. Qi, J. Zhou, J. Zhou, B. Hu and W. Chen, *Nano Energy*, 2013, **2**, 1071-1078.

13 L. Yuan, X. Xiao, T. Ding, J. Zhong, X. Zhang, Y. Shen, B. Hu, Y. Huang, J. Zhou and Z. L. Wang, *Angew. Chem. Int. Ed.*, 2012, **124**, 5018-5022.

14 A. K. Geim and K. S. Novoselov, *Nat. Mater.*, 2007, **6**, 183-191.

15 A. K. Geim, *Science*, 2009, **324**, 1530-1534.

16 K. S. Kim, Y. Zhao, H. Jang, S. Y. Lee, J. M. Kim, K. S. Kim, J.-H. Ahn, P. Kim, J.-Y. Choi and B. H. Hong, *Nature*, 2009, **457**, 706-710.

17 A. L. M. Reddy, A. Srivastava, S. R. Gowda, H. Gullapalli, M. Dubey and P. M. Ajayan, *ACS Nano*, 2010, **4**, 6337-6342.

18 M. J. Allen, V. C. Tung and R. B. Kaner, *Chem. Rev.*, 2009, **110**, 132-145.

19 X. Wang, Y. Zhang, C. Zhi, X. Wang, D. Tang, Y. Xu, Q. Weng, X. Jiang, M. Mitome, D. Golberg and Y. Bando, *Nat. Commun.*, 2013, **4**.

20 Z. Weng, Y. Su, D.-W. Wang, F. Li, J. Du and H.-M. Cheng, *Adv. Energy Mater.*, 2011, **1**, 917-922.

21 S. Pei, J. Zhao, J. Du, W. Ren and H.-M. Cheng, *Carbon*, 2010, **48**, 4466-4474.

22 M. Wang, L. D. Duong, J.-S. Oh, N. T. Mai, S. Kim, S. Hong, T. Hwang, Y. Lee and J.-D. Nam, *ACS Appl. Mat. Interfaces*, 2014, **6**, 1747-1753.

23 K. Rana, S. D. Kim and J.-H. Ahn, *Nanoscale*, 2015.

24 W. S. Hummers and R. E. Offeman, *JACS*, 1958, **80**, 1339-1339.

25 M. Zhu, W. Meng, Y. Huang, Y. Huang and C. Zhi, *ACS Appl. Mat. Interfaces*, 2014, **6**, 18901-18910.

26 B. Shen, W. Zhai and W. Zheng, *Adv. Funct. Mater.*, 2014, **24**, 4542-4548.

27 G. Xin, H. Sun, T. Hu, H. R. Fard, X. Sun, N. Koratkar, T. Borca-Tasciuc and J. Lian, *Adv. Mater.*, 2014, **26**, 4521-4526.

28 C. Chen, Q.-H. Yang, Y. Yang, W. Lv, Y. Wen, P.-X. Hou, M. Wang and H.-M. Cheng, *Adv. Mater.*, 2009, **21**, 3007-3011.

29 D.-W. Wang, F. Li, J. Zhao, W. Ren, Z.-G. Chen, J. Tan, Z.-S. Wu, I. Gentle, G. Q. Lu and H.-M. Cheng, *ACS Nano*, 2009, **3**, 1745-1752.

30 G. Eda, G. Fanchini and M. Chhowalla, *Nat. Nanotech.*, 2008, **3**, 270-274.

31 J. Che, L. Shen and Y. Xiao, *J. Mater. Chem.*, 2010, **20**, 1722-1727.

32 C. Mattevi, G. Eda, S. Agnoli, S. Miller, K. A. Mkhoyan, O. Celik, D. Mastrogiovanni, G. Granozzi, E. Garfunkel and M. Chhowalla, *Adv. Funct. Mater.*, 2009, **19**, 2577-2583.

33 A. Gupta, G. Chen, P. Joshi, S. Tadigadapa and Eklund, *Nano Lett.*, 2006, **6**, 2667-2673.

34 A. C. Ferrari, J. C. Meyer, V. Scardaci, C. Casiraghi, M. Lazzeri, F. Mauri, S. Piscanec, D. Jiang, K. S. Novoselov, S. Roth and A. K. Geim, *Phys. Rev. Lett.*, 2006, **97**, 187401.

35 D. P. Dubal, J. G. Kim, Y. Kim, R. Holze, C. D. Lokhande and W. B. Kim, *Energy Technology*, 2014, **2**, 325-341.

36 W. Meng, W. Chen, L. Zhao, Y. Huang, M. Zhu, Y. Huang, Y. Fu, F. Geng, J. Yu, X. Chen and C. Zhi, *Nano Energy*, 2014, **8**, 133-140.

37 L. Hu, W. Chen, X. Xie, N. Liu, Y. Yang, H. Wu, Y. Yao, M. Pasta, H. N. Alshareef and Y. Cui, *ACS Nano*, 2011, **5**, 8904-8913.

38 L.-B. Kong, M. Liu, J.-W. Lang, Y.-C. Luo and L. Kang, *J. Electrochem. Soc.*, 2009, **156**, A1000-A1004.

39 R. Liu and S. B. Lee, *JACS*, 2008, **130**, 2942-2943.

40 J. Liu, L. Zhang, H. B. Wu, J. Lin, Z. Shen and X. W. Lou, *Energy Environ. Sci.*, 2014, **7**, 3709-3719.

41 T. Cottineau, M. Toupin, T. Delahaye, T. Brousse and D. Bélanger, *Appl. Phys. A*, 2006, **82**, 599-606.

42 M. F. El-Kady, V. Strong, S. Dubin and R. B. Kaner, *Science*, 2012, **335**, 1326-1330.

43 X. Lu, G. Wang, T. Zhai, M. Yu, S. Xie, Y. Ling, C. Liang, Y. Tong and Y. Li, *Nano Lett.*, 2012, **12**, 5376-5381.

44 X. Lu, M. Yu, G. Wang, T. Zhai, S. Xie, Y. Ling, Y. Tong and Y. Li, *Adv. Mater.*, 2013, **25**, 267-272.

45 L. Yuan, X.-H. Lu, X. Xiao, T. Zhai, J. Dai, F. Zhang, B. Hu, X. Wang, L. Gong, J. Chen, C. Hu, Y. Tong, J. Zhou and Z. L. Wang, *ACS Nano*, 2011, **6**, 656-661.
46 H.-Q. Wang, Z.-S. Li, Y.-G. Huang, Q.-Y. Li and X.-Y. Wang, *J. Mater. Chem.*, 2010, **20**, 3883-3889.
47 H. Jiang, C. Li, T. Sun and J. Ma, *Nanoscale*, 2012, **4**, 807-812.